

Strain-Correlated Localized Exciton Energy in Atomically Thin Semiconductors

Hyowon Moon, Eric Bersin, Chitrleema Chakraborty, Ang-Yu Lu, Gabriele Grosso, Jing Kong, and Dirk Englund*

Cite This: *ACS Photonics* 2020, 7, 1135–1140

Read Online

ACCESS |

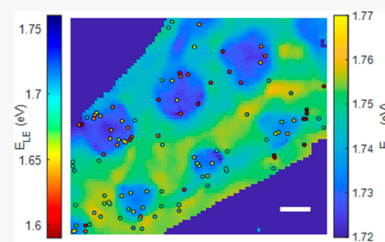
Metrics & More

Article Recommendations

Supporting Information

ABSTRACT: Single-photon emitters represent a key component for many quantum technologies, from quantum communication to computation. Atomically thin two-dimensional materials are promising hosts of quantum emitters, thanks to great freedom in assembling atomically precise heterostructures that are suitable for chip integration. Recent work showed that stable quantum emitters can be positioned deterministically by placing a 2D material over protrusions in a substrate. However, the origins of these emitters and their broad spectral distribution remain unclear. It has been suggested that the microscopic strain modulation near the protrusions plays a role because of local band gap modulation and band realignment, but the precise relationship between local strain and the transition energy of the quantum emitter remains elusive. To tackle this problem, we study free and localized excitons in a monolayer of WSe_2 transferred onto microstructures. These measurements show positive correlation between the localized emission energies and the strain-modulated free-exciton energies. Moreover, their energy separation is larger than 42 meV, in agreement with recent theory suggesting that the quantum emitters originate from local strain-mediated mixing of dark exciton states and highly localized atomic defect states. Our results open the potential for deterministic positioning and spectral control of quantum emitters in 2D material heterostructures.

KEYWORDS: 2D materials, tungsten diselenide, single-photon emitters, local strain engineering



Quantum emitters in solids have applications ranging from single-photon sources to spin-photon interfaces^{1–3} to quantum sensors.⁴ The recent discovery of single-photon emitters (SPEs) in atomically thin 2D materials, such as insulating hexagonal boron nitride (hBN)^{5–7} and semiconducting transition metal dichalcogenides (TMDs),^{8–12} has opened new possibilities for atomic-precision imaging and positioning as well as new types of heterostructures that would be difficult or impossible in bulk materials.¹³ Moreover, SPEs can be created by applying local strain on WS_2 and WSe_2 ,^{14–19} making them promising candidates for scalable integration into systems on chip. Recent works have integrated SPEs in WSe_2 with plasmonic metal nanostructures^{20–24} and into photonic circuits.^{25,26}

However, controlling the emission energies of such emitters has proved to be more difficult than controlling their positions. It has been shown that nanopillars with equal diameter are associated with a random number of emitters per site and that these emitters can have widely distributed emission energies over 100 meV, even for very small structures of 100 nm size.^{16,20} Tuning of emission energy has been demonstrated through applying an out-of-plane electric field²⁷ or in-plane strain,^{28,29} but the tuning range of 2–20 meV is much smaller than the inhomogeneous distribution of the emission energy. Also, the local in-plane strain applied to WSe_2 structures has only been simulated rather than experimentally measured.^{28,29}

On the other hand, there have been experimental and theoretical efforts to attribute emitter creation in these systems to the intrinsic defect-state³⁰ or the combination of strain and intrinsic defects.³¹ In this work, we elucidate the role of strain by a careful study of the emission energy of bright localized emitters hosted by atomically thin WSe_2 , along with its relationship to the local strain induced by microstructures. Our measurements show a strong positive relation between localized emission energy and experimentally measured local strain. Moreover, we find that nearly all localized excitons emit at least 42 meV below the free-exciton energy. This energy difference matches the energy difference between bright and dark excitons in WSe_2 measured to be 42^{32,33} to 47 meV.^{34–36} This result supports a recent theory that associates the origin of SPEs with the hybridization of strain-confined intervalley (dark) excitons and defect excitons.³¹ In addition, we find that the lower-energy emission occurs where strain is higher at the edges, corners, and areas of high surface roughness in our

Received: April 18, 2020

Published: April 29, 2020



structures, as confirmed by atomic force microscopy (AFM) and scanning electron microscopy (SEM).

Figure 1a shows an optical microscope image of a $50 \times 10 \mu\text{m}^2$ monolayer WSe₂ flake transferred onto a SiO₂ substrate,

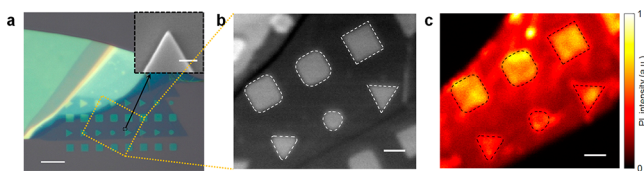


Figure 1. (a) Optical microscope image of the WSe₂ flake transferred onto the SiO₂ substrate with protruded structures. The monolayer covers many of the triangular- and square-shaped structures (the scale bar is $10 \mu\text{m}$). Inset shows the corner of the sharpest structure of 15 nm radius; the scale bar is 100 nm . (b) Confocal laser reflection scan and (c) photoluminescence map of the yellow-dashed region of (a) at 4 K (the scale bar is $1 \mu\text{m}$). Overlaid white and black dashed lines in (b) and (c) represent the outlines of the structures.

which is patterned with microstructures of different shapes made of hydrogen silsesquioxane (HSQ) (see Methods). The triangular- and square-shaped structures have a height of 50 nm and an edge length of $2 \mu\text{m}$ with radii of curvature swept from 0 to 500 nm in the mask design. The lithography-limited radius of curvature is about 15 nm , as seen in Figure 1a, inset (see Figure S1 for details). We performed confocal spectro-

scopy measurements at 4 K in a closed cycle cryostat. Figure 1b shows a confocal laser reflection image of the $8.4 \times 7.2 \mu\text{m}^2$ yellow-dashed region (R1) in Figure 1a. The corresponding photoluminescence (PL) map clearly shows the monolayer WSe₂ region in Figure 1c. We then produced a hyperspectral image by recording PL spectra at low excitation power (8 nW , 6.5 W/cm^2) across this region in steps of 100 nm .

Resolving the PL image into a narrower spectral band ($1647 \pm 0.2 \text{ meV}$) reveals a spatially localized bright emitter (E1) at the corner of the structure, as shown in Figure 2a. Figure 2b plots the spectrum of the emitter E1 as a red line, revealing a narrow emission feature. A second-order autocorrelation measurement of this peak, with bandpass filtering across $1642\text{--}1653 \text{ meV}$ (red shaded region), indicates that this bright emission is mostly due to a single photon emitter as $g^{(2)}(0) = 0.27 < 0.5$. The spectrum of the nearby position labeled as BG (black line) shows only a weak and broad feature. The hyperspectral image reveals many similar bright spots distinguished by sharp spectral peaks akin to Figure 2a. Two other exemplary emitters around 1604 meV are shown in Figure S2. Next, we systematically find all the peaks from the entire region of interest. To exclude the effect of the noise and broadband background features from finding sharp peaks, we applied a binning for nearby two pixels in each direction and high-pass-filter (HPF) to the spectra with a 3 dB cutoff at 0.11 meV^{-1} . Figure 2c shows the PL map from Figure 2a with this

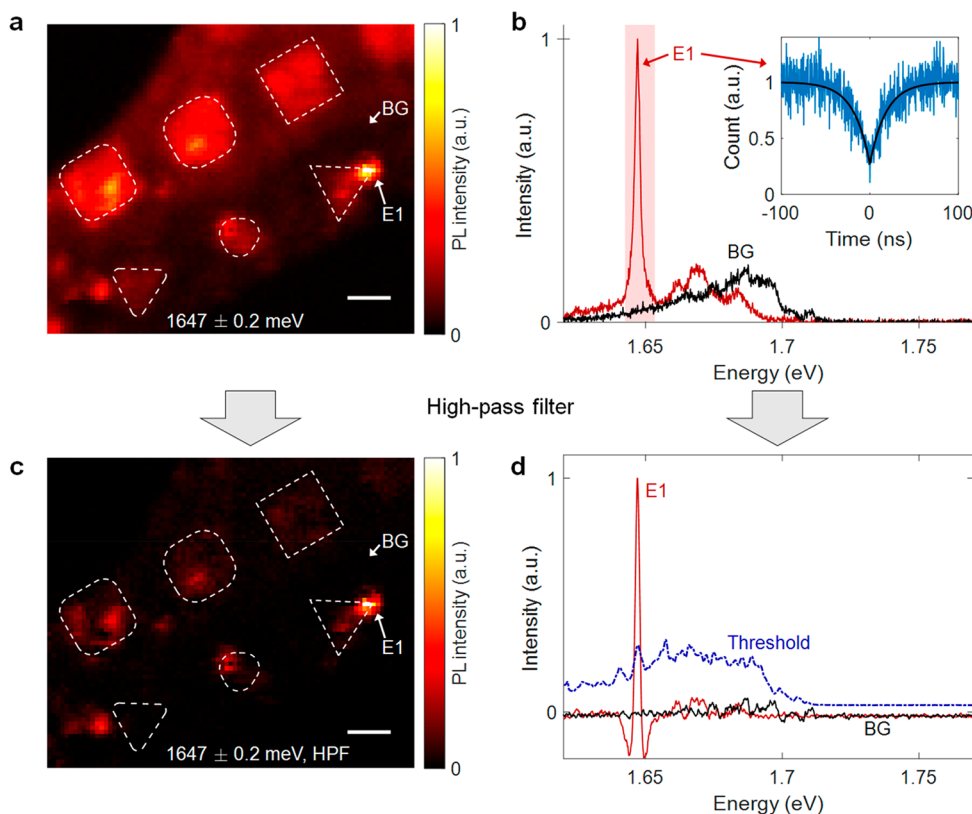


Figure 2. (a) Spectrally filtered PL map of $1647 \pm 0.2 \text{ meV}$ shows the creation of a bright emitter at the corner of the triangular structure, labeled as E1. White dashed lines indicate the edges of the structures, and BG indicates a position without bright emitters. The scale bar is $1 \mu\text{m}$. (b) PL spectra at the position of the emitter E1 (red) and background position BG (black). Both spectra show a broad and weak localized band, while E1 shows a sharp peak on top of it. The single-photon nature of E1 is confirmed by a second-order autocorrelation measurement (inset) taken with spectral filters (red shaded region). (c) High-pass-filtered PL map of the same spectral range as in (a). Background signals are mostly gone inside the structure. The scale bar is $1 \mu\text{m}$. (d) High-pass-filtered spectra at the positions of E1 (red) and BG (black) show that the weak and broad localized bands are suppressed effectively. The blue dashed line indicates a threshold value at each energy ($\text{thres}(E) = \text{mean}(E) + 7 \text{ std}(E)$).

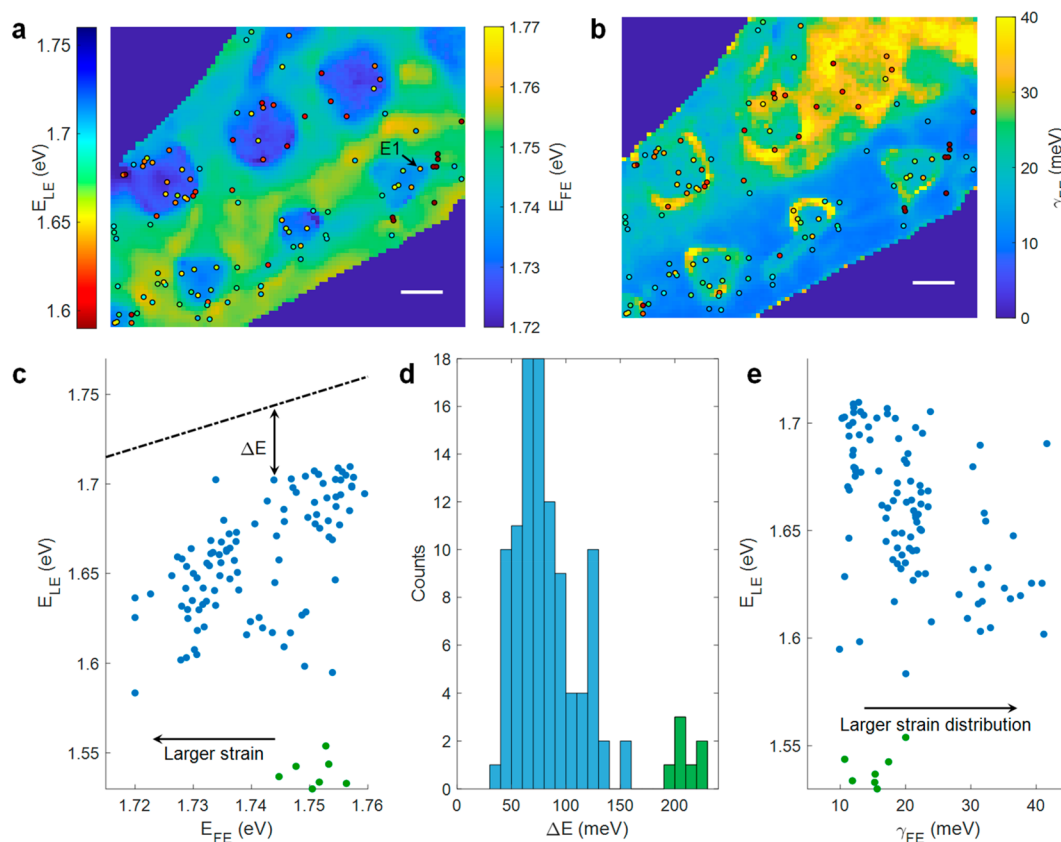


Figure 3. (a) Location and color-coded emission energy of 108 localized emitters (E_{LE} , left color bar) which is overlaid onto the free-exciton peak energy (E_{FE} , right color bar) map measured with high-power excitation. The free-exciton peak energy red shifts as there is stronger tensile strain. The map shows the average strain value on the top surface of the structure is higher than that of outside due to the rougher surface, consistent with AFM measurements as shown in Figure 4a. The scale bar is $1\ \mu\text{m}$. (b) Same color-coded dots overlaid onto spatial distribution map of the fwhm line width (γ_{FE}) of the free-exciton peak. The line width broadens when the strain within the diffraction-limited spot is strongly inhomogeneous, especially at the edges and corners of the structures. The scale bar is $1\ \mu\text{m}$. (c) The emission energy of localized emitters (E_{LE}) versus the free-exciton energy (E_{FE}) measured at the same position. The confinement energy ($\Delta E = E_{FE} - E_{LE}$) can be calculated for all the emitters. (c–e) Distinguishable group of deep-confined emitters, mostly hosted at the folds, are plotted as green. (d) Histogram of ΔE between the free-exciton energy and the localized emission shows the cutoff energy. (e) Emission energy of the localized emitters (E_{LE}) versus the fwhm of the free-exciton peak (γ_{FE}). The negative correlation implies the large local strain distribution is important to host deep-level emissions.

filter applied, and Figure 2d shows the filtered spectra at the positions of E1 and BG. Both show suppression of a spectrally broad localized band. Then we choose bright emitters whose peak intensity is higher than a threshold, which is chosen to be 7 standard deviations above the mean value of the entire filtered map at the peak energy ($I_{\text{peak}}(E) > \text{mean}(E) + 7\ \text{std}(E)$), shown as a blue dashed line in Figure 2d. A total of 108 emitters were found, with their locations overlaid in Figure 3a and b as color-coded dots which represent their emission energy (E_{LE}). The locations and peak energy of all the emitters are listed in Table S1.

Biaxial tensile strain loaded on WSe_2 monolayers red shifts the free-exciton energy by $60\ \text{meV}/\%$.^{37,38} We use this relationship to estimate the magnitude of local strain across the sample by measuring the free-exciton energy as a function of spatial coordinates. To increase the free-exciton spectral weight, we acquire a hyperspectral image of the same region at high excitation power ($3.5\ \mu\text{W}$, $2.8\ \text{kW}/\text{cm}^2$). At this power, excitons saturate the localized states, resulting in strong intensity at the free-exciton band in most of the region. The free-exciton band energy (E_{FE}) and full-width half-maximum (fwhm) line width (γ_{FE}) at each position are extracted by fitting a Gaussian function and plotted in Figure 3a and b,

respectively. Red shift, and thus strain, is larger on top of the HSQ structures compared to the Si/SiO_2 substrate. We attribute this to the difference in surface roughness, as discussed in detail in the following paragraph and Figure S3. The line width of the free-exciton band at 4 K, shown in Figure 3b, represents the inhomogeneous distribution of the local strain within the optically resolvable spot.³⁹ Large inhomogeneity of strain, characterized by broader line width, highlights the edges of the structures due to the large height difference.

The effect of strain on the quantum emission energy is further studied by correlating two energies. Figure 3c plots the energy of localized emitters (E_{LE}) versus the free-exciton energy (E_{FE}). The black line is a guide to eye that shows free-exciton energy ($E_{LE} = E_{FE}$), and the confinement energy (ΔE) can be calculated for each emitter by subtracting one from the other ($\Delta E = E_{FE} - E_{LE}$). A histogram of ΔE is plotted in Figure 3d with a bin size of 10 meV. With the exception of a single emitter found at a highly strained region, the confinement energy is larger than 42 meV. This value is very similar to the energy difference between dark and bright excitons at zero-strain level,^{32–35} supporting a recently suggested theory that dark excitons play a role in the formation of single-photon emitters in WSe_2 .³¹ The histogram also shows

that most of the emission occurs between 40–140 meV below the strain-shifted free-exciton energy value at the position (group 1). However, there is clearly distinguishable group (group 2) at even lower energies ($\Delta E > 199$ meV), mostly hosted at a material wrinkle that can create extremely localized strain and a multilayer environment due to folding of the monolayer. There is a positive correlation of 0.267 between the E_{FE} and E_{LE} for all measured emitters, which increases to 0.610 when we exclude the extremely confined group 2 emitters. Figure 3e shows that E_{FE} tends to decrease when the strain distribution is large such that the line width of free-exciton emission is broader.

AFM and SEM measurements help to investigate the distribution of strain and the origin of the emitters with higher spatial resolution. AFM measurements in Figure 4a

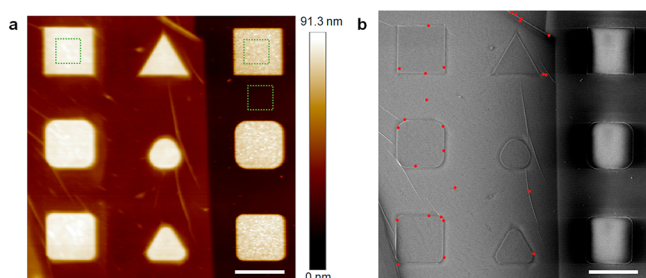


Figure 4. SEM and AFM measurements. (a) AFM image of the same region reveals detailed structure and roughness. Green dotted squares indicate the region where the average surface roughness is measured, giving rise to surface roughnesses (R_a) of 0.22, 1.2, and 0.53 nm for bare SiO_2 surface, bare HSQ structure, and WSe_2 transferred onto the HSQ structures, respectively. (b) SEM image of the region of interest with overlaid red dots ($E_{FE} < 1.63$ eV) indicating deep-confined emitters. Most of the emitters are hosted near the corners of the structures or where the wrinkle meets the edges of the structures. The scale bars are 2 μm .

reveal the surface roughnesses (R_a) of 0.22, 1.2, and 0.53 nm for the bare SiO_2 surface, the bare HSQ structure, and the WSe_2 transferred onto the HSQ structures, respectively. The large strain in WSe_2 on the HSQ structures compared to SiO_2 can be attributed to the difference in the roughness of the substrate. The SEM image in Figure 4b shows wrinkles and foldings induced by the transfer process in the same sample region. The red dots overlaid in Figure 4b show the locations of deeply confined emitters whose energy is lower than 1.63 eV. These deep emissions occur at the corners and edges of the structures. Indeed, SEM images with higher magnification (Figure S4) show that the sharp or rounded corners host wrinkles in the monolayer, which can be a crucial step to confine zero-dimensional excitons along the edges of the structure. A similar effect is expected in nanopillar structures and could explain why there are multiple quantum emitters per pillar along the edges. On the whole, these experiments based on strain-induced optical responses, SEM and AFM indicate that the emitter spatial distribution can be attributed to variations of the local strain in the sample. Similar measurements and analysis on a different region of the sample (R2) indicate that the effect of the geometry is reproducible (Figure S5 and S6).

In conclusion, we have characterized the relationship between local strain and emission energy of localized emitters hosted in atomically thin semiconductors. The localized

emission energies show positive correlation to the strain-modulated free-exciton energy at the same positions, with the offset energy of 42 meV being similar to the energy difference between bright and dark excitons in WSe_2 . Our result supports the theory which attributes the origin of quantum emission in TMDs to the mixing of strain-confined intervalley excitons with intrinsic defect excitons.³¹ Moreover, deep-confined emissions mostly occur at the edges and corners of the structures, suggesting the local wrinkles as possible causes of zero-dimensional exciton confinement in nanostructures. Further studies of the effect of local strain on the antibunching behavior and associated lifetimes would facilitate the scalable control of the localized emitters. The observed relationship between local strain and SPE emission energy and the good agreement with theory elucidate the origin of strain-associated SPEs in 2D materials, opening the door to large-scale creation of site- and frequency-controlled quantum emitters.

METHODS

Device Fabrication. Structures were fabricated by spinning 4% hydrogen silsesquioxane (HSQ) at 6000 rpm for 1 min, resulting in a resist thickness of 52 nm. The structures were written via electron-beam lithography with an exposure of 16 mC/cm² and developed in salt solution comprising 1 wt % NaOH and 4 wt % NaCl for 3 min. An exfoliated monolayer WSe_2 flake was directly transferred onto these structures.

Optical Characterization. All the optical measurements were done with a home-built confocal microscopy setup at 4 K in a cryostat (Montana Instruments). The narrow-band (<1 MHz) excitation laser (M2 SolsTiS EMM) was tuned at 633 nm for low-power (8 nW) and high-power (3.5 μW) hyperspectral imaging. Spectra with low-power excitation were averaged by the nearby 2 pixels in each direction to remove artificial peaks from noise and high-pass-filtered to find sharp peaks from broad localized band, as described in the main text. The analyzed bright emitters are with the peak intensity higher than 7 standard deviations from the mean value of the entire map at the peak energy ($I_{\text{peak}}(E) > \text{mean}(E) + 7 \text{std}(E)$). Spectra with high-power measurement were similarly high-pass-filtered to reduce the effect of localized bands, and then free-exciton peaks were fitted by a Gaussian function to extract peak energy and line width.

ASSOCIATED CONTENT

Supporting Information

The Supporting Information is available free of charge at <https://pubs.acs.org/doi/10.1021/acsp Photonics.0c00626>.

SEM images and locations of emitters, measurements on the other region, and full list of localized emitters (PDF)

AUTHOR INFORMATION

Corresponding Author

Dirk Englund – Department of Electrical Engineering and Computer Science, Massachusetts Institute of Technology, Cambridge, Massachusetts 02139, United States; orcid.org/0000-0002-1043-3489; Phone: 617-324-7014; Email: englund@mit.edu

Authors

Hyowon Moon – Department of Electrical Engineering and Computer Science, Massachusetts Institute of Technology, Cambridge, Massachusetts 02139, United States

Eric Bersin – Department of Electrical Engineering and Computer Science, Massachusetts Institute of Technology, Cambridge, Massachusetts 02139, United States; orcid.org/0000-0003-0643-5534

Chitrallema Chakraborty – Department of Electrical Engineering and Computer Science, Massachusetts Institute of Technology, Cambridge, Massachusetts 02139, United States; John A. Paulson School of Engineering and Applied Sciences, Harvard University, Cambridge, Massachusetts 02138, United States

Ang-Yu Lu – Department of Electrical Engineering and Computer Science, Massachusetts Institute of Technology, Cambridge, Massachusetts 02139, United States

Gabriele Grosso – Photonics Initiative, Advanced Science Research Center and Physics Program, Graduate Center, City University of New York, New York, New York 10031, United States; orcid.org/0000-0002-2577-1755

Jing Kong – Department of Electrical Engineering and Computer Science, Massachusetts Institute of Technology, Cambridge, Massachusetts 02139, United States; orcid.org/0000-0003-0551-1208

Complete contact information is available at:
<https://pubs.acs.org/10.1021/acsp Photonics.0c00626>

Notes

The authors declare no competing financial interest.

ACKNOWLEDGMENTS

This work was supported in part by the Army Research Office (ARO) Multidisciplinary University Research Initiative (MURI) program, grant no. W911NF-18-1-0431, and in part by National Science Foundation (NSF) Research Advanced by Interdisciplinary Science and Engineering (RAISE), grant no. CHE-1839155. H.M. acknowledges support by Samsung Scholarship. E.B. was supported by a NASA Space Technology Research Fellowship and the NSF Center for Ultracold Atoms (CUA).

REFERENCES

- (1) Aharonovich, I.; Englund, D.; Toth, M. Solid-State Single-Photon Emitters. *Nat. Photonics* **2016**, *10*, 631–641.
- (2) Atatüre, M.; Englund, D.; Vamivakas, N.; Lee, S.-Y.; Wrachtrup, J. Material Platforms for Spin-Based Photonic Quantum Technologies. *Nat. Rev. Mater.* **2018**, *3* (5), 38–51.
- (3) Awschalom, D. D.; Hanson, R.; Wrachtrup, J.; Zhou, B. B. Quantum Technologies with Optically Interfaced Solid-State Spins. *Nat. Photonics* **2018**, *12* (9), 516–527.
- (4) Degen, C. L.; Reinhard, F.; Cappellaro, P. Quantum Sensing. *Rev. Mod. Phys.* **2017**, *89* (3), 035002.
- (5) Tran, T. T.; Bray, K.; Ford, M. J.; Toth, M.; Aharonovich, I. Quantum Emission from Hexagonal Boron Nitride Monolayers. *Nat. Nanotechnol.* **2016**, *11* (1), 37–41.
- (6) Grosso, G.; Moon, H.; Lienhard, B.; Ali, S.; Efetov, D. K.; Furchi, M. M.; Jarillo-Herrero, P.; Ford, M. J.; Aharonovich, I.; Englund, D. Tunable and High-Purity Room Temperature Single-Photon Emission from Atomic Defects in Hexagonal Boron Nitride. *Nat. Commun.* **2017**, *8* (1), 705.
- (7) Proscia, N. V.; Shotan, Z.; Jayakumar, H.; Reddy, P.; Cohen, C.; Dollar, M.; Alkauskas, A.; Doherty, M.; Meriles, C. A.; Menon, V. M. Near-Deterministic Activation of Room-Temperature Quantum Emitters in Hexagonal Boron Nitride. *Optica* **2018**, *5*, 1128.
- (8) Srivastava, A.; Sidler, M.; Allain, A. V.; Lembke, D. S.; Kis, A.; Imamoglu, A. Optically Active Quantum Dots in Monolayer WSe₂. *Nat. Nanotechnol.* **2015**, *10*, 491–496.
- (9) He, Y.-M.; Clark, G.; Schaibley, J. R.; He, Y.; Chen, M.-C.; Wei, Y.-J.; Ding, X.; Zhang, Q.; Yao, W.; Xu, X.; et al. Single Quantum Emitters in Monolayer Semiconductors. *Nat. Nanotechnol.* **2015**, *10*, 497–502.
- (10) Koperski, M.; Nogajewski, K.; Arora, A.; Cherkez, V.; Mallet, P.-Y.; Veuillen, J.; Marcus, J.; Kossacki, P.; Potemski, M. Single Photon Emitters in Exfoliated WSe₂ Structures. *Nat. Nanotechnol.* **2015**, *10*, 503–506.
- (11) Chakraborty, C.; Kinnischtzke, L.; Goodfellow, K. M.; Beams, R.; Vamivakas, A. N. Voltage-Controlled Quantum Light from an Atomically Thin Semiconductor. *Nat. Nanotechnol.* **2015**, *10*, 507–511.
- (12) Tonndorf, P.; Schmidt, R.; Schneider, R.; Kern, J.; Buscema, M.; Steele, G. A.; Castellanos-Gomez, A.; van der Zant, H. S. J.; de Vasconcellos, S. M.; Bratschitsch, R. Single-Photon Emission from Localized Excitons in an Atomically Thin Semiconductor. *Optica* **2015**, *2*, 347.
- (13) Geim, A. K.; Grigorieva, I. V. Van der Waals Heterostructures. *Nature* **2013**, *499* (7459), 419–425.
- (14) Kumar, S.; Kaczmarczyk, A.; Gerardot, B. D. Strain-Induced Spatial and Spectral Isolation of Quantum Emitters in Mono- and Bilayer WSe₂. *Nano Lett.* **2015**, *15* (11), 7567–7573.
- (15) Branny, A.; Kumar, S.; Proux, R.; Gerardot, B. D. Deterministic Strain-Induced Arrays of Quantum Emitters in a Two-Dimensional Semiconductor. *Nat. Commun.* **2017**, 15053.
- (16) Palacios-Berraquero, C.; Kara, D. M.; Montblanch, A. R.-P.; Barbone, M.; Latawiec, P.; Yoon, D.; Ott, A. K.; Loncar, M.; Ferrari, A. C.; Atatüre, M. Large-Scale Quantum-Emitter Arrays in Atomically Thin Semiconductors. *Nat. Commun.* **2017**, *8*, 15093.
- (17) Rosenberger, M. R.; Dass, C. K.; Chuang, H.-J.; Sivaram, S. V.; McCreary, K. M.; Hendrickson, J. R.; Jonker, B. T. Quantum Calligraphy: Writing Single-Photon Emitters in a Two-Dimensional Materials Platform. *ACS Nano* **2019**, *13*, 904–912.
- (18) Kern, J.; Niehues, I.; Tonndorf, P.; Schmidt, R.; Wigger, D.; Schneider, R.; Stiehm, T.; Michaelis de Vasconcellos, S.; Reiter, D. E.; Kuhn, T.; et al. Nanoscale Positioning of Single-Photon Emitters in Atomically Thin WSe₂. *Adv. Mater.* **2016**, *28* (33), 7101–7105.
- (19) Rodt, S.; Reitzenstein, S.; Heindel, T. Deterministically Fabricated Solid-State Quantum-Light Sources. *J. Phys.: Condens. Matter* **2020**, *32* (15), 153003.
- (20) Luo, Y.; Shepard, G. D.; Ardelean, J. V.; Rhodes, D. A.; Kim, B.; Barmak, K.; Hone, J. C.; Strauf, S. Deterministic Coupling of Site-Controlled Quantum Emitters in Monolayer WSe₂ to Plasmonic Nanocavities. *Nat. Nanotechnol.* **2018**, *13*, 1137–1142.
- (21) Iff, O.; Lundt, N.; Betzold, S.; Tripathi, L. N.; Emmerling, M.; Tongay, S.; Lee, Y. J.; Kwon, S.-H.; Höfling, S.; Schneider, C. Deterministic Coupling of Quantum Emitters in WSe₂ Monolayers to Plasmonic Nanocavities. *Opt. Express* **2018**, *26*, 25944.
- (22) Luo, Y.; Liu, N.; Li, X.; Hone, J. C.; Strauf, S. Single Photon Emission in WSe₂ up to 160 K by Quantum Yield Control. *2D Mater.* **2019**, *6*, 035017.
- (23) Cai, T.; Dutta, S.; Aghaeimeibodi, S.; Yang, Z.; Nah, S.; Fourkas, J. T.; Waks, E. Coupling Emission from Single Localized Defects in Two-Dimensional Semiconductor to Surface Plasmon Polaritons. *Nano Lett.* **2017**, *17* (11), 6564–6568.
- (24) Cai, T.; Kim, J.-H.; Yang, Z.; Dutta, S.; Aghaeimeibodi, S.; Waks, E. Radiative Enhancement of Single Quantum Emitters in WSe₂ Monolayers Using Site-Controlled Metallic Nanopillars. *ACS Photonics* **2018**, *5*, 3466–3471.
- (25) White, D.; Branny, A.; Chapman, R. J.; Picard, R.; Brotons-Gisbert, M.; Boes, A.; Peruzzo, A.; Bonato, C.; Gerardot, B. D. Atomically-Thin Quantum Dots Integrated with Lithium Niobate Photonic Chips [Invited]. *Opt. Mater. Express* **2019**, *9*, 441.

(26) Peyskens, F.; Chakraborty, C.; Muneeb, M.; Van Thourhout, D.; Englund, D. Integration of Single Photon Emitters in 2D Layered Materials with a Silicon Nitride Photonic Chip. *Nat. Commun.* **2019**, *10* (10), 4435.

(27) Chakraborty, C.; Goodfellow, K. M.; Dhara, S.; Yoshimura, A.; Meunier, V.; Vamivakas, A. N. Quantum-Confined Stark Effect of Individual Defects in a van der Waals Heterostructure. *Nano Lett.* **2017**, *17*, 2253–2258.

(28) Iff, O.; Tedeschi, D.; Martín-Sánchez, J.; Moczala-Dusanowska, M.; Tongay, S.; Yumigeta, K.; Taboada-Gutiérrez, J.; Savaresi, M.; Rastelli, A.; Alonso-González, P.; et al. Strain-Tunable Single Photon Sources in WSe₂ Monolayers. *Nano Lett.* **2019**, *19* (10), 6931–6936.

(29) Chakraborty, C.; Mukherjee, A.; Moon, H.; Konthasinghe, K.; Qui, L.; Hou, W.; Pena, T.; Watson, C.; Wu, S. M.; Englund, D.; Vamivakas, N. Strain-Tuning of the Emission Axis of Quantum Emitters in an Atomically Thin Semiconductor. *Optica* **2020**, accepted.

(30) Dass, C. K.; Khan, M. A.; Clark, G.; Simon, J. A.; Gibson, R.; Mou, S.; Xu, X.; Leuenberger, M. N.; Hendrickson, J. R. Ultra-Long Lifetimes of Single Quantum Emitters in Monolayer WSe₂/hBN Heterostructures. *Adv. Quantum Technol.* **2019**, *2*, 1900022.

(31) Linhart, L.; Paur, M.; Smejkal, V.; Burgdörfer, J.; Mueller, T.; Libisch, F. Localized Intervalley Defect Excitons as Single-Photon Emitters in WSe₂. *Phys. Rev. Lett.* **2019**, *123* (14), 146401.

(32) Zhou, Y.; Scuri, G.; Wild, D. S.; High, A. A.; Dibos, A.; Jauregui, L. A.; Shu, C.; De Greve, K.; Pistunova, K.; Joe, A. Y.; et al. Probing Dark Excitons in Atomically Thin Semiconductors via near-Field Coupling to Surface Plasmon Polaritons. *Nat. Nanotechnol.* **2017**, *12* (9), 856–860.

(33) Li, Z.; Wang, T.; Jin, C.; Lu, Z.; Lian, Z.; Meng, Y.; Blei, M.; Gao, S.; Taniguchi, T.; Watanabe, K.; et al. Emerging Photoluminescence from the Dark-Exciton Phonon Replica in Monolayer WSe₂. *Nat. Commun.* **2019**, *10* (1), 1–7.

(34) Zhang, X.-X.; Cao, T.; Lu, Z.; Lin, Y.-C.; Zhang, F.; Wang, Y.; Li, Z.; Hone, J. C.; Robinson, J. A.; Smirnov, D.; et al. Magnetic Brightening and Control of Dark Excitons in Monolayer WSe₂. *Nat. Nanotechnol.* **2017**, *12* (9), 883–888.

(35) Molas, M. R.; Faugeras, C.; Slobodeniuk, A. O.; Nogajewski, K.; Bartos, M.; Basko, D. M.; Potemski, M. Brightening of Dark Excitons in Monolayers of Semiconducting Transition Metal Dichalcogenides. *2D Mater.* **2017**, *4* (2), 021003.

(36) Mueller, T.; Malic, E. Exciton Physics and Device Application of Two-Dimensional Transition Metal Dichalcogenide Semiconductors. *npj 2D Mater. and Appl.* **2018**, *29*.

(37) Schmidt, R.; Niehues, I.; Schneider, R.; Drüppel, M.; Deilmann, T.; Rohlfing, M.; de Vasconcellos, S. M.; Castellanos-Gomez, A.; Bratschitsch, R. Reversible Uniaxial Strain Tuning in Atomically Thin WSe₂. *2D Mater.* **2016**, *3*, 021011.

(38) Frisenda, R.; Druppel, M.; Schmidt, R.; Michaelis de Vasconcellos, S.; Perez de Lara, D.; Bratschitsch, R.; Rohlfing, M.; Castellanos-Gomez, A. Biaxial Strain Tuning of the Optical Properties of Single-Layer Transition Metal Dichalcogenides. *npj 2D Mater. Appl.* **2017**, *10*.

(39) Moon, H.; Grosso, G.; Chakraborty, C.; Peng, C.; Taniguchi, T.; Watanabe, K.; Englund, D. Dynamic Exciton Funneling by Local Strain Control in a Monolayer Semiconductor. *arXiv (Mesoscale and Nanoscale Physics)*, June 24, 2019, ver. 1. <https://arxiv.org/abs/1906.10077>.